J Eng Math (2012) 73:17–30
DOI 10.1007/s10665-011-9485-1

The relation of steady evaporating drops fed by an influx and freely evaporating drops

Desislava Todorova · Uwe Thiele · Len M. Pismen

Received: 15 January 2010 / Accepted: 16 May 2011 / Published online: 9 June 2011

Abstract We discuss a thin film evolution equation for a wetting evaporating liquid on a smooth solid substrate. The model is valid for slowly evaporating small sessile droplets when thermal effects are insignificant, while wettability and capillarity play a major role. The model is first employed to study steady evaporating drops that are fed locally through the substrate. An asymptotic analysis focuses on the precursor film and the transition region towards the bulk drop and a numerical continuation of steady drops determines their fully non-linear profiles. Following this, we study the time evolution of freely evaporating drops without influx for several initial drop shapes. As a result we find that drops initially spread if their initial contact angle is larger than the apparent contact angle of large steady evaporating drops with influx. Otherwise they recede right from the beginning.

Keywords Capillarity · Drop · Disjoining pressure · Evaporation · Thin film equation · Wettability

1 Introduction

Evaporation of thin liquid films and sessile droplets has attracted much attention both as the way to probe the dynamics of the contact line [1,2] and as a route to create deposition patterns through sedimentation of solutes and suspensions [3–6]. A number of studies concentrate on problems pertinent to any evaporation process, which include mass and heat transfer and thermocapillarity [7,8]. For slowly evaporating small sessile droplets studied in contemporary well-controlled experiments on smooth surfaces [2,9], thermal effects are, however, insignificant, while contact line dynamics and liquid–substrate interactions play a major role. It has been suggested that the relation between spreading and evaporation/condensation goes both ways, so that the latter may alleviate the notorious contact line singularity [10,11]. For background on spreading see, e.g., [12,13].

D. Todorova (✉) · U. Thiele
Department of Mathematical Sciences, Loughborough University, Loughborough, LE11 3TU Leicestershire, UK
e-mail: d.todorova@lboro.ac.uk

U. Thiele
e-mail: u.thiele@lboro.ac.uk

L. M. Pismen
Department of Chemical Engineering and Minerva Center for Nonlinear Physics of Complex Systems,
Technion–Israel Institute of Technology, 32000 Haifa, Israel
e-mail: pismen@technion.ac.il

A remarkable phenomenon observed in evaporating completely wetting liquids is the formation of a dynamic meniscus with a finite contact angle [4,9,14]. The standard approach to computing the form of a spreading and evaporating drop and the resulting dynamic contact angle [8,15,16] is based on the lubrication approximation with the singularity at the contact line alleviated by slip. The evaporation rate is treated in three alternative ways. One possibility, realised in the presence of a temperature difference between the substrate and the vapour phase [8], is the evaporation rate determined by the balance of latent heat and heat flux. The evaporation rate is then uniform in the limit of small Biot numbers, but diverges near the contact line in the opposite limit. Both limits can also be realised under isothermal conditions. The evaporation rate is uniform (as long as the layer thickness remains outside the range of intermolecular forces) when evaporation is controlled either by phase transition kinetics at the interface or by diffusion through a boundary layer of constant thickness in a stirred vessel. If evaporation is diffusionally controlled with no stirring, the evaporation rate increases towards the contact line; an analytical solution based on interfacial equilibrium with no flux onto the unwetted substrate yields the flux diverging on the contact line [16,17]. Another approach accounts for the influence of the thermal conductivity of the substrate and the dependence of the vapour saturation concentration on temperature [18,19].

The aim of this article is to present a simple isothermal thin film evolution equation with evaporation limited by phase transition kinetics (or boundary layer transfer, but not diffusion) that correctly describes the influence of effective molecular interactions on evaporation in the case of complete wetting. This is achieved by taking into account the dependence of the saturated vapour pressure on the disjoining pressure and curvature in the way it has been done in studies of the dynamics of evaporating films [20–22] but not in the cited studies of droplet spreading. This allows us to describe in a consistent way the transition from the bulk droplet to a precursor layer and eliminate singularities at the contact line. Note, however, that our model may be obtained as the isothermal limit of the models in [7,23], i.e., letting the difference of substrate and ambient temperature, and the latent heat go to zero. It also corresponds to the limit of infinite thermal conductivity of the liquid.

Following [8,15], we consider a two-dimensional 'fed' system that allows us to study steady states of evaporating droplets. These steady states are compared to droplet shapes resulting from a time evolution of an evaporating droplet (without influx). The comparison will be employed to discuss a possible special role the steady-state profiles play in the time evolution. A related approach is taken in [24], where steady fronts of evaporating liquid on an incline are considered.

This article is structured as follows. Section 2 introduces our model and discusses the scaling, whereas Sect. 3 discusses the asymptotics in the precursor film. Section 4 discusses the properties of steady drops with influx as a function of the influx strength and of the single remaining dimensionless parameter. The time-evolution in the case without influx is analysed in Sect. 5 where we also compare the steady drop profiles in the case with influx to the time-dependent profiles in the non-fed case. Section 6 gives our conclusions.

2 Basic model and scaling

For simplicity, we restrict our attention to a two-dimensional system as sketched in Fig. 1. Conceptually, there exists no difference to the full three-dimensional system, we only expect the transport rates to change.

Using the lubrication approximation, the evaporation dynamics for an isothermal droplet of liquid on a porous substrate is captured by an evolution equation for the film thickness profile h [20,22,25,26]

$$\partial_t h = -\partial_x\, j_{\mathrm{conv}}(x) - j_{\mathrm{evap}}(x) + q(x), \tag{1}$$

$$j_{\mathrm{conv}}(x) = -\frac{h^3}{3\eta}\,\partial_x p, \quad j_{\mathrm{evap}}(x) = \beta\left(\frac{p}{\rho} - \mu_0\right),$$

$$p = -\gamma\,\partial_{xx} h - \Pi(h). \tag{2}$$

The first and second terms on the r.h.s. of Eq. 1 are the divergence of the convective flux $j_{\mathrm{conv}}(x)$ and the evaporative flux $j_{\mathrm{evap}}(x)$, which correspond, respectively, to the conserved and non-conserved part of the dynamics. The function $q(x)$ is the influx through the (locally) porous substrate. The evaporative flux is proportional to the

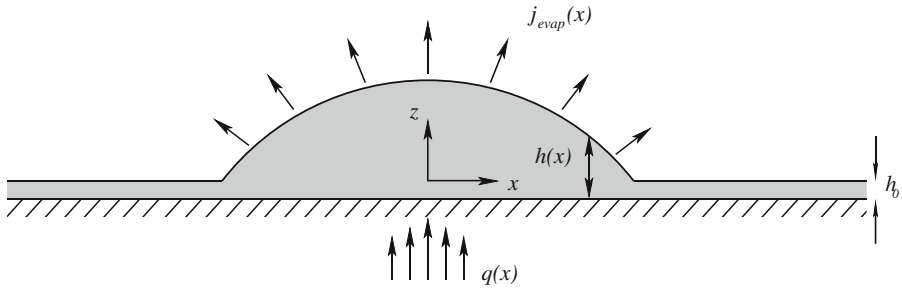

Fig. 1 Sketch of the two-dimensional geometry employed for investigating an evaporating droplet with localised influx $q(x)$

difference between the chemical potential of the ambient vapour and the chemical potential in the liquid $\mu = p/\rho$; p is pressure, β is an effective evaporation rate constant; and γ, ρ and η are the surface tension, mass density and dynamic viscosity of the liquid, respectively. The pressure p contains the curvature pressure $-\gamma\partial_{xx}h$ and the disjoining pressure $\Pi(h)$ modelling wettability [12,25,27–29]; the hydrostatic pressure is neglected as we focus on nano- and micro-droplets.

To model a droplet of completely wetting liquid, we employ a long-range stabilising van der Waals disjoining pressure $\Pi = -A/6\pi h^3$ with the Hamaker constant $A < 0$ [20,26,28,30–32]. Note that other sign conventions are also common (cf. e.g., [12,27,33]). The model (1) is related to various models in the literature: it may be obtained from the one in [20] by adding an influx and replacing the disjoining pressure for a partially wetting liquid by one for a wetting liquid. The models in [7,23] incorporate various thermal aspects that are here neglected by assuming that the latent heat is very small or/and the thermal conductivity is very large. The same applies to the steady-state description in [34]. Note that our model also corresponds to the one in [23] in the limit of zero superheat.

A dimensionless form of Eqs. 1 and 2 can be obtained by choosing the characteristic energy density of molecular interactions between the fluid and the substrate $\kappa = |A|/6\pi h_0^3$ as the pressure scale and the equilibrium film thickness $h_0 = |A/6\pi\rho\mu_0|^{1/3}$ corresponding to the ambient vapour potential μ_0 as the scale of film thickness h (note that $\mu_0 < 0$ when a thick flat film evaporates). The horizontal coordinate x and time t can be scaled in several ways [22]. A short horizontal length scale

$$l = \sqrt{\frac{\gamma h_0}{\kappa}} = h_0^2\sqrt{\frac{6\pi\gamma}{|A|}} = \left(\frac{|A|}{6\pi}\right)^{1/6}\frac{\sqrt{\gamma}}{|\rho\mu_0|^{2/3}} \tag{3}$$

is fixed by the balance between disjoining pressure and surface tension at the thickness of the wetting layer, and determines the extent of a region adjacent to the contact line where the interface may be strongly curved due to interaction with the substrate. The lubrication approximation remains formally applicable as long as l far exceeds h_0. Note, however, that lubrication approximation often still predicts the qualitative behaviour for many systems with larger contact angles [25,29]. When considering the results obtained with models like Eq. 1, one has to always keep in mind that even very large contact angles obtained in lubrication approximation (measured as slopes at the inflection point of the drop profiles) correspond to rather small angles in physical scaling.

Another horizontal scale, applicable in the precursor layer, is determined by the balance of flow driven by the disjoining pressure gradient and evaporation:

$$L = \sqrt{\frac{h_0^3\rho}{\beta\eta}} = \sqrt{\left|\frac{A}{6\pi\mu_0\beta\eta}\right|}, \tag{4}$$

This scale is large when evaporation is slow. It is appropriate to choose L as the horizontal scale, assuming it to be of the same order of magnitude as the third available scale—the droplet size. The respective time scale is $T = (L/h_0)^2\eta/\kappa$, and the flux j_{conv} is scaled by h_0L/T.

Retaining the same notation for the rescaled variables, we rewrite Eqs. 1 and 2 as

$$\partial_t h = -\partial_x j_{\rm conv}(x) + \left(\epsilon\, \partial_{xx} h + \frac{1}{h^3} - 1\right) + q(x), \tag{5}$$

$$j_{\rm conv}(x) = \frac{h^3}{3}\partial_x \left(\epsilon\, \partial_{xx} h + \frac{1}{h^3}\right), \tag{6}$$

where the parameter

$$\epsilon = \frac{(6\pi)^{2/3}\gamma\beta\eta}{|A|^{2/3}\rho^{4/3}|\mu_0|^{1/3}} \tag{7}$$

denotes the scale ratio $(l/L)^2$. Note that it is proportional to the evaporation rate constant β, but contains as well a weak dependence on the chemical potential μ_0 in the denominator.

In the following, we will study steady-state droplets that are obtained for an influx $q(x)$ localised at the centre of the drop (Sect. 4). Below, the steady profiles are compared to time simulations without influx for different initial profiles (Sect. 5). First, however, we discuss the asymptotics in the precursor film.

3 Asymptotics in the precursor film

In the outer precursor region, the film is almost flat and surface tension can be neglected, i.e., we set $\epsilon = 0$ in Eqs. 5 and 6 and assume $q(x) = 0$. In the linear regime the film thickness decays exponentially to its equilibrium value $h = 1$:

$$h - 1 \sim \exp(-\sqrt{3}x). \tag{8}$$

Note the difference from the non-physical asymptotics $h \sim x^{1/4}$ in [16] where the dependence of the evaporation equilibrium on the disjoining pressure was neglected. The latter profile corresponds to the well-known result of de Gennes [27] who failed to recognise it as an *unstable* solution.

To discuss the nonlinear behaviour we reduce Eqs.5 and 6 to the stationary equation

$$\frac{{\rm d}^2 \ln h}{{\rm d}x^2} = 1 - \frac{1}{h^3}. \tag{9}$$

This equation is solved by using h as an independent variable, and $y(h) = ({\rm d}\ln h/{\rm d}x)^2$ as a dependent variable. The transformed equation is

$$y'(h) = \frac{2}{h}\left(1 - \frac{1}{h^3}\right). \tag{10}$$

It is integrated with the boundary condition $y(1) = 0$ to yield

$$y(h) = 2\left[\ln h - \frac{1}{3}\left(1 - \frac{1}{h^3}\right)\right]. \tag{11}$$

The precursor film profile is obtained in an implicit form

$$\sqrt{2}x = \int \left[H - \frac{1}{3}\left(1 - e^{-3H}\right)\right]^{-1/2} {\rm d}H, \tag{12}$$

where $H = \ln h$. This solution formally implies a very fast growth $h \sim \exp[(x - x_0)^2]$ towards the bulk of the droplet. It becomes, however, inapplicable as h grows, necessitating a modified scaling. One can see that the two terms in the r.h.s. of Eq. 6 become, up to logarithmic corrections, comparable at $h \sim \epsilon^{-1/4}$, which, though appreciably exceeding the thickness of the equilibrium wetting layer $h = 1$, may be still far below the height of the bulk droplet. As follows from Eq. 11, the incline at this thickness level is, up to logarithmic corrections, $h_x = h\sqrt{y(h)} \sim \epsilon^{-1/4}$

in agreement with results by Morris [34,35]. This sheds light on the origin of a finite contact angle in an evaporating droplet. As we will in Sect. 4 the numerically obtained dependence agrees well with the asymptotic result.

The flux J from the droplet bulk into the precursor at a 'transitional' location X corresponding to the thickness level $h = \epsilon^{-1/4}\zeta$ is determined by the total evaporation rate from the precursor, which can be obtained directly from Eq. 9:

$$J = \int_X^\infty \left(1 - \frac{1}{h(x)^3}\right) \mathrm{d}x = -\left(\frac{\mathrm{d}\ln h}{\mathrm{d}x}\right)_{x=X} \approx \sqrt{2\left(\ln\frac{\zeta}{\epsilon^{1/4}} - \frac{1}{3}\right)}. \tag{13}$$

The dependence both on ϵ and on a precise choice of the level ζ is very weak. The rest of evaporation goes at an almost constant rate from the bulk of a large droplet.

4 Steady-state droplets with influx

For zero influx through the porous substrate ($q(x) = 0$) the only steady-state solution is $h = h_0$. However, for $q(x) \neq 0$ steady droplets may exist with a volume determined by the dynamic equilibrium between the overall influx through the substrate and the overall evaporation flux.

Here, we use continuation techniques [36–38] to numerically analyse the steady-state solutions of Eqs. 5 and 6, i.e., we set $\partial_t h = 0$ and solve the resulting ordinary differential equation as a boundary value problem on a domain of size D with the boundary conditions (for a symmetrical drop) $\partial_x h = \partial_{xxx} h = 0$ at $x = 0$ (drop centre). At $x = D$ we employ either $h = 1$ and $\partial_x h = 0$, or $\partial_x h = 0$ and $\partial_{xx} h = 0$. If the domain is sufficiently large the results depend neither on the particular choice of D nor on the used version of boundary conditions at $x = D$. For details on the usage of continuation methods for thin film equations see, e.g., [39–41] where they have been employed to study sliding drops, chemically driven running drops and drops pinned by wettability defects, respectively.

For the influx $q(x)$ we use a normalised Gaussian

$$q(x) = q_0 \frac{2}{\sigma\sqrt{\pi}} \exp\left[-\frac{x^2}{\sigma^2}\right] \tag{14}$$

with $q_0 = \int_0^\infty q(x)\,\mathrm{d}x$ being the total influx through the substrate. If the droplet size is large as compared to the width σ, the results do not depend on the particular choice of σ.

Figures 2 and 3 show profiles of rather small (nano-)droplets (left panels) and the corresponding dependencies of the evaporative flux on position (right panels). The results are given for various moderate values of the influx q_0 (Fig. 2) and the length scale ratio ϵ (Fig. 3). In all shown cases these droplets are not much higher than the wetting layer. For such small drops the behaviour is dominated by the influence of the disjoining pressure. In consequence,

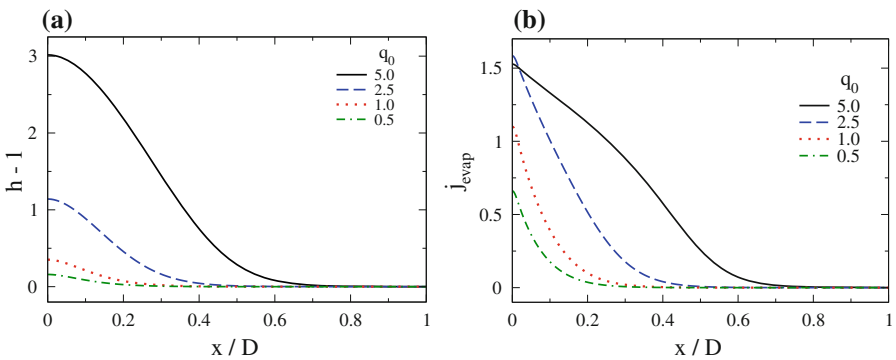

Fig. 2 (colour online) For the case of small droplets, we give **a** droplet profiles and **b** evaporation flux in dependence of position for $\epsilon = 1.0$ and various total influxes q_0 as given in the legend. Domain size is $D = 10$ and $\sigma = 0.1$

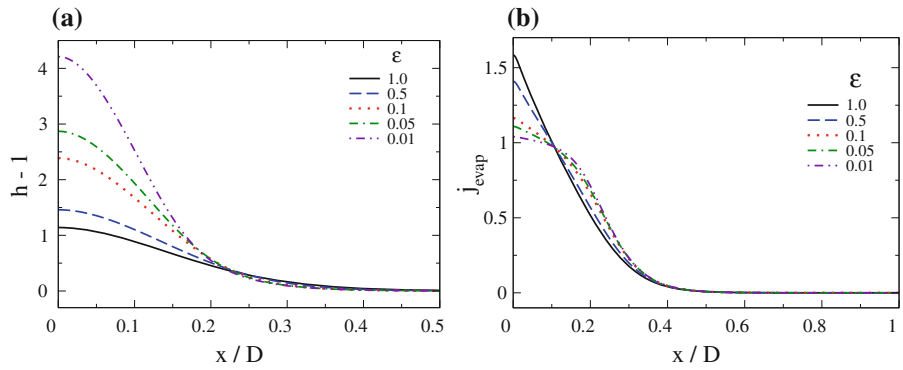

Fig. 3 (colour online) For the case of small droplets, we show **a** droplet profiles and **b** evaporation flux in dependence of position for $q_0 = 2.5$ and various ϵ as given in the legend. Domain size is $D = 10$ and $\sigma = 0.1$

the evaporation decreases monotonically from the centre of the drops towards the contact region. Interestingly, in all cases the droplet assumes a shape that does not allow for any condensation of liquid even in the contact line region where the Laplace pressure is negative. Note that there exists a one-to-one correspondence between the strength of the influx q_0 and droplet volume for fixed ϵ. This implies that one may characterise the relative size of droplets either by volume or by influx q_0.

For extremely small drops (see, e.g., profile for $q_0 = 0.5$ in Fig. 2) the disjoining pressure influence is stronger than the capillary pressure even at the drop centre. As a result, the absolute value of the evaporation flux j_{evap} is smaller than one even at the centre of the drop. For slightly larger drops (see, e.g., profile for $q_0 = 2.5$ in Fig. 2) the capillary pressure dominates the disjoining pressure at the drop centre and j_{evap} is larger than one. With a further increase in drop size the influence of the capillary pressure diminishes and j_{evap} eventually approaches unity everywhere with the exception of the contact line region (cf. Fig. 4).

Decreasing ϵ mainly influences the height of the droplets while the width remains roughly constant (Fig. 3a). This implies that the curvature at the drop centre and the apparent contact angle θ_{app} (defined as the maximal slope of the drop profile), increase with decreasing ϵ. However, although curvature increases we find that the influence of capillarity on the evaporation flux decreases (Fig. 3b). For $\epsilon = 0.01$, one has at the drop centre j_{evap} slightly above one. Furthermore, at the same ϵ, j_{evap} has already a small plateau at the drop centre, i.e., the flux is nearly constant at the value determined solely by the chemical potential.

The influence of the source width σ is marginal as long as it is sufficiently smaller than the droplet width. For moderately large width it has still no influence on the contact line region but has some influence on the centre of the drop. Increasing, for instance, σ from 0.1 to 1.0 at constant $j_0 = 2.5$ and $\epsilon = 1$ the drop volume goes up by about 5%. Decreasing σ down to 0.001 has no visible influence on the droplet shape.

The droplets discussed up to this point represent nano-droplets of heights normally below 500 nm. However, for much smaller ϵ or much larger q_0 one is able to study micro-droplets with heights in the 10–100 µm range. Figure 4 shows profiles of such drops and the local evaporative flux for $\epsilon = 10^{-6}$. For such large drops the local evaporation is essentially constant for the 'bulk drop' and decreases monotonically in a confined contact region (Fig. 4b). Figure 4c shows the logarithm of $h - 1$. By shifting the drops in the x-direction one can appreciate that the approach to $h = 1$ is universal and well described by the linear relation $h - 1 \sim \exp(-\sqrt{3}x)$ derived above (see Eq. 8 in Sect. 3).

When increasing the influx for fixed ϵ the steady drops become larger in width and height (Fig. 2a). This is indicated as well by the dependence of volume on influx (Fig. 5a). The corresponding apparent contact angle is shown in Fig. 5b. One clearly distinguishes a small- and a large-drop regime with a crossover at about $V = 1$. In the small-drop regime, volume and contact angle are both proportional to the influx. In the large-drop regime, the contact angle approaches a constant (or increases with growing influx following a power law with an exponent smaller than 1/5), whereas the volume depends quadratically on influx. The latter is easily explained noticing that

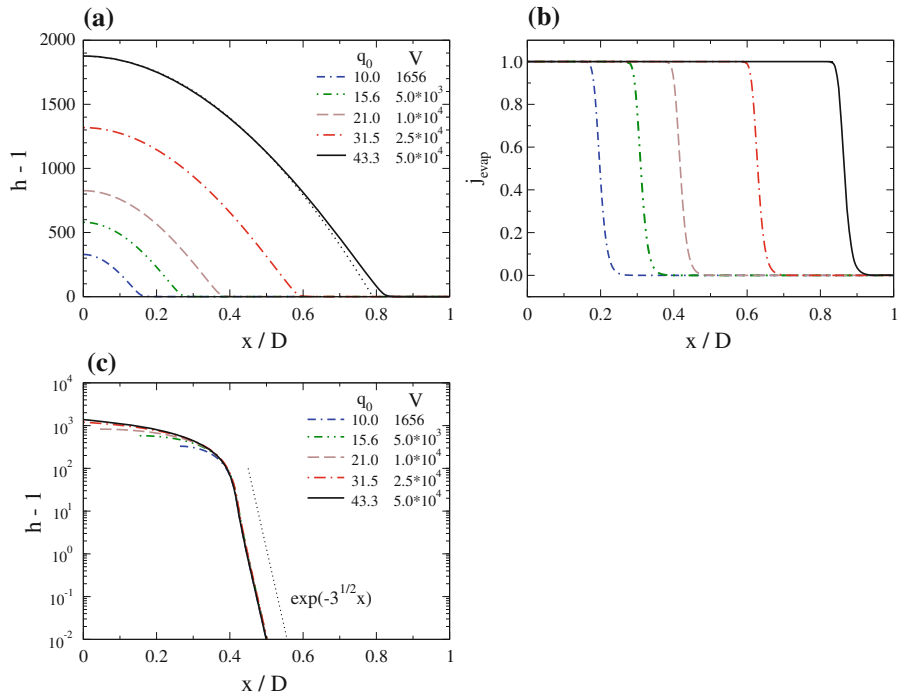

Fig. 4 (colour online) For the case of large drops, we show for $\epsilon = 10^{-6}$ **a** drop profiles and **b** evaporation flux in dependence of position. Results are given for various total influxes j_0 and droplet volumes V (see legend). The *thin dotted line* in (**a**) gives for the largest drop the corresponding parabolic drop profile of identical maximal height and curvature at centre (corresponding to a spherical cap in lubrication approximation). Panel **c** shows $\log h$ to indicate the universal behaviour near the contact line (drops shifted in x). The *dotted line* indicates the linear result $h - 1 \sim \exp(-\sqrt{3}x)$ (Eq. 8). Domain size is $D = 50$ and $\sigma = 0.1$

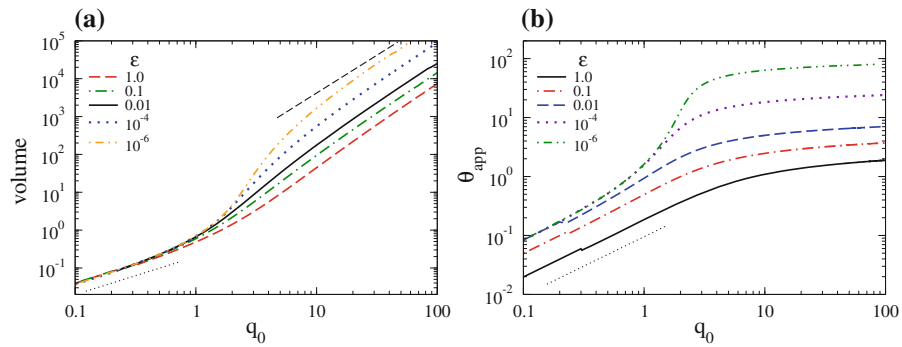

Fig. 5 Shown are **a** drop volume and **b** the apparent contact angle θ_{app} (defined as the maximal slope of the drop profile), in dependence of total influx q_0 for various length scale ratios ϵ as given in the legend. The *straight dotted* [*dashed*] lines indicate linear [quadratic] dependencies, respectively

the evaporative outflux for large drops is proportional to the surface 'area' of the drop (negligible influence of Laplace and disjoining pressure). For a constant contact angle the area under the parabola depends quadratically on its arc length. For the influx to balance the outflux, the surface area has to grow proportionally with the influx, i.e., the volume increases quadratically with the influx.

Inspecting Fig. 5 further, one notices that the overall behaviour is different for larger ($\epsilon \gtrsim 10^{-3}$) and smaller ($\epsilon \lesssim 10^{-3}$) drops. In the former case, the transition between the small- and the large-drop regime is monotonic,

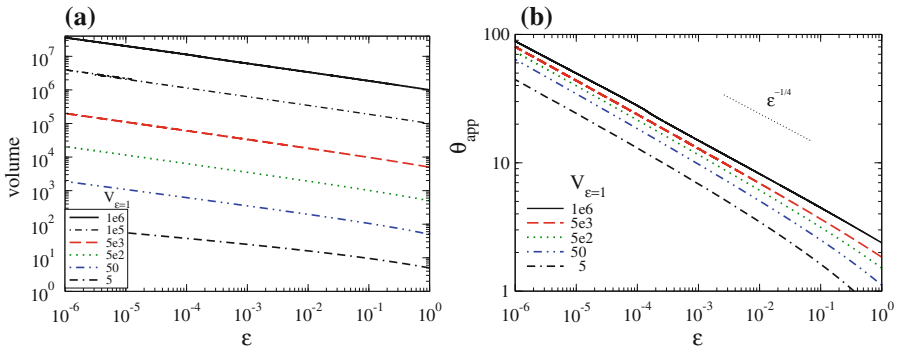

Fig. 6 (colour online) Shown are **a** drop volume and **b** apparent contact angle in dependence of the length scale ratio ϵ. The total influx q_0 is constant for each line, respectively. The lines are characterised by the drop volume at $\epsilon = 1.0$ (see legends)

i.e., the slopes of the curves in Fig. 5 change monotonically. In contrast, for small $\epsilon \lesssim 10^{-3}$ in the transition range one may define a third region where the slopes of the $V(q_0)$ and $\theta_{\text{app}}(q_0)$ curves pass through a maximum.

The tendency towards a constant contact angle for increasing volume can also be observed in Fig. 6a and b where we plot the drop volume and the apparent contact angle, respectively, as a function of the length scale ratio ϵ for various fixed influxes for rather large drops. We find that for large drops, the volume as well as the contact angle decrease for increasing length scale ratio ϵ roughly as $\epsilon^{-1/4}$. This agrees with the asymptotic expression determined above in Sect. 3.

For smaller drops, deviations from the power law are found at larger ϵ. Interestingly, the dependence of the contact angle on ϵ seems to approach a limiting curve for large drops. In the following, we employ the curve for the largest drops in Fig. 3 as an approximation to the asymptotic dependence of θ_{app} on ϵ for infinitely large drops.

5 Time evolution without influx

Next, we study the time evolution of evaporating droplets without influx through the substrate, i.e., we simulate Eq. 5 with $q(x) = 0$. The domain size D and boundary conditions at $x = 0$ and $x = D$ correspond to the ones used in the steady-state calculations in the previous section. We use three different initial profiles $h_i(x) = h(x, t = 0)$ of equal maximal height h_{m} and volume V: (i) a parabola $h_i(x) = (h_{\text{m}} - 1)(1 - x/x_c)^2 + 1$ with $x_c = 3V/(h_{\text{m}} - 1)$ for $0 \le x \le x_c$ and $h_i(x) = 1$ for $x > x_c$; (ii) a gaussian $h_i(x) = (h_{\text{m}} - 1)\exp((x/\sigma)^2) + 1$ with $\sigma = 2V/\sqrt{\pi}(h_{\text{m}} - 1)$; and (iii) the steady-state solution of identical V and h_{m} obtained in section 4.

Figure 7 shows a space–time plot for a typical time evolution observed when using an initial parabolic drop profile that has the same height and volume as a fed drop obtained in Sect. 4. The case shown is for $\epsilon = 10^{-4}$. At early

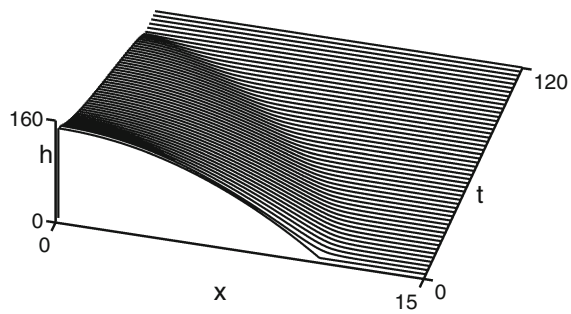

Fig. 7 Space–time plot of an evaporating droplet for $\epsilon = 10^{-4}$. The initial profile is a parabola on a precursor film of thickness $h_{\text{p}} = 1$. It has a volume of $V = 1000$ and maximal height of $H_{\text{max}} = 140.6$. The corresponding contact angle is $\theta_{\text{ini}} = 26.3$. The initial height corresponds to the one at $V = 1000$ for the steady-state drops with influx for the corresponding ϵ (obtained in Sect. 4)

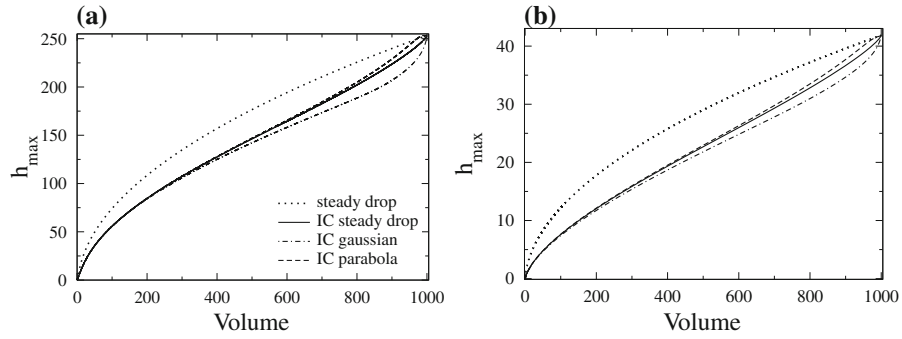

Fig. 8 Trajectories in the phase plane spanned by the maximal drop height and drop volume for **a** $\epsilon = 10^{-6}$ and **b** $\epsilon = 1$. Shown are curves resulting from (i) time evolutions for three different initial profiles of equal maximal height and volume (parabola, gaussian, and steady state with influx) and (ii) calculations of steady-state solutions with influx as obtained by continuation

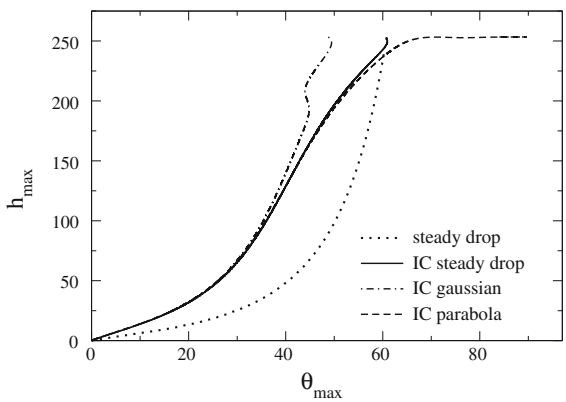

Fig. 9 Trajectories in the phase plane spanned by the maximal drop height and apparent contact angle for $\epsilon = 10^{-6}$. Cases shown correspond to the ones in Fig. 8a

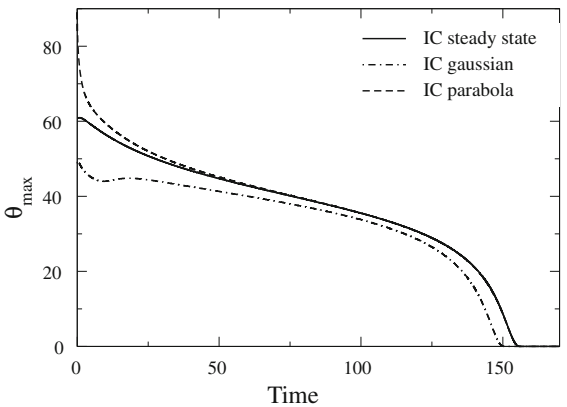

Fig. 10 Shown is the dependence of the apparent contact angle on time for $\epsilon = 10^{-6}$. The given cases correspond to the three evaporating drops in Fig. 8a

times the contact line region relaxes under the influence of the disjoining pressure, thereby decreasing the apparent contact angle. Subsequently, the width and height of the drop decrease monotonically until at about $T = 100$ the drop has vanished and only the stable precursor film remains. When starting (as in the present case) with the drop measures (volume and height) as obtained for the drop with influx, the evolution always looks similar. In particular, we have not found that the drop macroscopically spreads at the beginning (by 'macroscopic' we mean a spreading that goes beyond the small local relaxation at the contact line).

A more complete picture of the time evolution for different initial profiles is obtained by considering the dependence of overall measures on time, and the trajectories of time evolutions in various 'phase planes'. For the axes of the latter we choose measures that do not change when the domain size is varied for an identical drop. We give results in two such phase planes, namely, the one spanned by volume and maximal drop height (Fig. 8) and the one spanned by maximal drop height and apparent contact angle (Fig. 9). The change of the contact angle over time is given in Fig. 10, whereas Fig. 11 shows selected drop profiles. Figure 8a and b compare results for very small $\epsilon = 10^{-6}$ and the largest used $\epsilon = 1$. As the results are qualitatively rather similar, the remaining Figs. 9, 10 and 11 are for $\epsilon = 10^{-6}$ only.

Scrutinising Figs. 8, 9, 10 and 11 one makes several observations: (i) the time evolutions starting from the three different initial profiles converge after some initial adjustments whose details depend on the particular initial profile shape. (ii) The convergence is slightly faster for smaller ϵ. Here, 'faster' means that the trajectories approach each

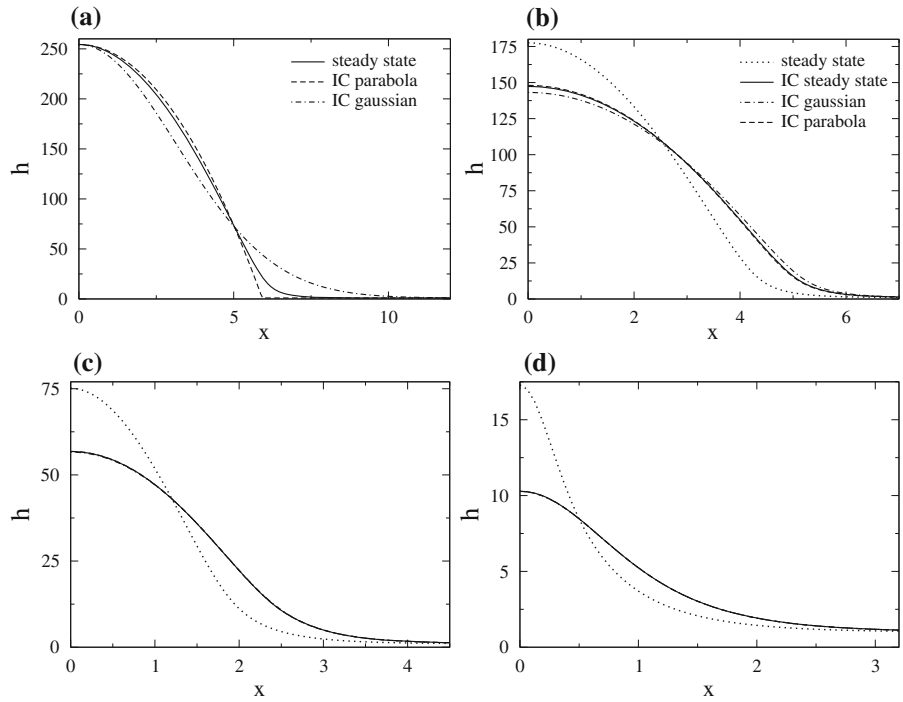

Fig. 11 Given are for $\epsilon = 10^{-6}$ drop profiles for selected drop volumes during the course of evaporation (for the three different initial profiles). We show as well the steady-state drop of the same volume. Panel **a** gives the initial profiles at $V = 1000$, whereas panels **b**, **c** and **d** show profiles at $V = 500$, $V = 100$ and $V = 10$, respectively

other at higher volume (cf. Fig. 8). In absolute terms the overall evolution becomes faster with increasing ϵ. Thereby, the trajectories of the initial parabola and the initial profile taken from the steady-state calculations approach each other earlier than they are approached by the trajectory of the initial gaussian. (iii) The family of steady profiles with influx represents drops clearly distinct from the 'freely evaporating' shrinking drops. The family of steady profiles does not approach the trajectories of evaporating profiles when the drops become small. Even for very small drops their contact angle remains always larger by a roughly constant factor than the one of the evaporating drops. The factor is about two for $\epsilon = 10^{-6}$ and approaches four for $\epsilon = 1$. (iv) The overall picture in Fig. 8 for different ϵ looks very similar, only the $h_{\max}$ axes scale differently. A similar observation holds for the representations as given in Figs. 9, 10 and 11 where, however, both axes would need to be scaled.

Next, we discuss the behaviour of the different initial drop profiles at early times. We use Fig. 9 as an example. For larger ϵ the behaviour is slightly less pronounced, but all the curves look qualitatively the same (not shown). For instance, one obtains a plot that is roughly the one for $\epsilon = 1$ when scaling the $h_{\max}$-axis and θ_{app}-axis of Fig. 9 by factors of 1/6 and 1/40, respectively. A similar rule applies to Fig. 10, when additionally scaling time by about 1/5. In Figs. 9 and 10, one finds for the initial parabola profile a strong decrease in the apparent contact angle at early times. This corresponds to an adjustment of the contact line region to the influences of the disjoining pressure. As the central drop region nearly coincides with the initial steady profile (per definition at same volume and height) the two curves approach each other rather fast. In the course of the time evolution the central part of the profile remains a parabola. However, for the gaussian at early times the contact angle changes non-monotonically: the profile adjusts, on the one hand, its contact line region to the disjoining pressure influences (related to the 'earlier wiggle' in the curve for the parabola in Fig. 9). On the other hand, its central region adapts to a parabola (second 'wiggle' in the curve in Fig. 9).

All three profiles approach each other after the initial adjustments. Their central part can be well fitted by a parabola, e.g., for $V = 500$ [$V = 100$] and $\epsilon = 10^{-6}$ down to thicknesses of about $h = 60$ [$h = 35$]. Keeping the

drop volume constant, that thickness decreases with increasing ϵ and vice versa. In contrast, the steady profile of the drop with influx can be fitted by a parabola in a smaller central part of the drop. The deviation from the parabola becomes clearly visible, e.g., for $V = 500$ [$V = 100$] and $\epsilon = 10^{-6}$ at about $h = 120$ [$h = 60$] (already 20–30% below the maximum). This percentage range remains roughly the same when changing ϵ for fixed drop volume.

Our direct comparison of evaporating steady-state drops with influx and evaporating drops without influx shows that the former cannot be used to approximate the latter as their shapes always differ. A freely evaporating shrinking drop has always a smaller apparent contact angle than the steady fed drop. This has been shown for a wide range of length scale ratios from $\epsilon = 10^{-6}$ to $\epsilon = 1$. Note, however, that the differences slowly decrease for decreasing ϵ.

We have observed that freely evaporating drops with a similar initial geometry (volume and height) as per steady-state drops, for the range of ϵ explored, never spread macroscopically before their contact line recedes. However, an initial spreading phase is often observed in experiments [9,12,14]. To investigate this further we perform a number of simulations starting with large parabolic drops. Figure 12 gives a set of space time plots obtained for different length scale ratios from $\epsilon = 10^{-6}$ to $\epsilon = 1$. All of them start from the identical initial profile. For small $\epsilon \lesssim 10^{-3}$ [panels a and b] the behaviour is very similar to the one described above for drops with the same initial geometry as the steady drops: the drops shrink monotonically, their height and width decrease slowly. However, at larger $\epsilon \gtrsim 10^{-3}$ [panels c and d] the behaviour is qualitatively different: At early times the drops spread. Thereby they loose height and gain width quite fast, the apparent contact angle decreases strongly. Then the drop reaches a maximal width before the contact line starts to recede again. In the shrinking stage, the height and width of the drop decrease slowly as before. The spreading is faster for larger ϵ (Fig. 12d).

The contact angle for the initial profile is in all cases $\theta_{\text{ini}} = 20.8$. Comparing this with Fig. 6b one notices that this angle roughly coincides with the limiting contact angle (for large drops) for $\epsilon \approx 3 \times 10^{-4}$. This value lies between the regions (in ϵ) where we find receding and spreading evaporating drops, respectively. Extrapolating from this finding, we formulate the hypothesis that the steady-state drops with influx studied in Sect. 4 represent limiting solutions between the case of spreading and shrinking freely evaporating drops (without influx).

To test the hypothesis we perform a number of time simulations with parabolic initial drops of different initial contact angle and at different ϵ. All of them are of the same (large) volume. The results are given as a scatter plot in Fig. 13 together with the curve for the large steady drops obtained in Sect. 4 (solid line of Fig. 6b). For each initial condition we record whether the drop spreads initially or directly starts to recede. Our results indicate that the above

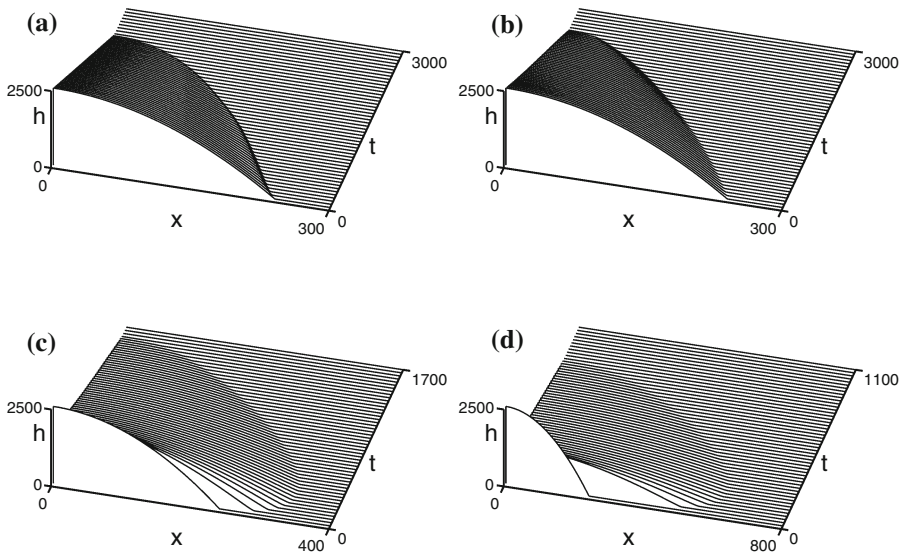

Fig. 12 Space–time plots of evaporating droplets for **a** $\epsilon = 10^{-6}$, **b** $\epsilon = 10^{-4}$, **c** $\epsilon = 10^{-2}$ and **d** $\epsilon = 1.0$. The initial profile is always the same parabola of maximal height $H_{\max} = 2500$ and volume 4×10^5 on a precursor film of $h = 1$. The corresponding contact angle is $\theta_{\text{ini}} = 20.8$

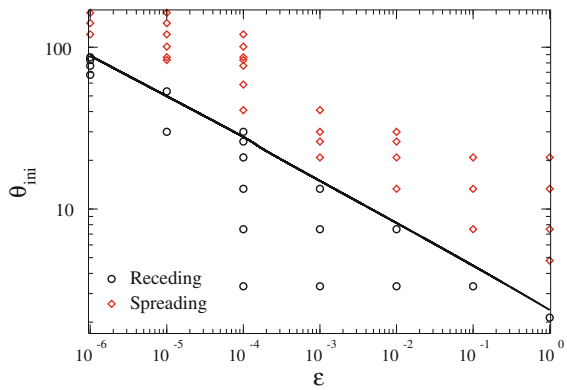

Fig. 13 (colour online) Phase diagram indicating the initial behaviour of an evaporating drop. In the plane spanned by the initial contact angle θ_{ini} and the length scale ratio ϵ we indicate where the drop initially spreads, and where the contact line recedes right from the beginning. Each *symbol* corresponds to a time simulation. The *solid line* corresponds to the numeric result characterising the large steady drops with influx (cf. Fig. 6b)

hypothesis seems to hold. The transition between initial spreading for large initial contact angle and a receding of the contact region right from the beginning roughly coincides with the power law dependence $\theta \sim \epsilon^{-1/4}$ (Fig. 6b, curve for large volume) not only in the power but as well in the prefactor. The prefactor of the curve obtained from the steady drops with influx seems to be slightly below the transition found in the time simulations. Further studies will be necessary to give a more detailed account.

6 Conclusions

We have analysed a thin film evolution equation for a wetting evaporating liquid on a smooth solid substrate. We have focused on slowly evaporating small sessile droplets where thermal effects are insignificant. Employing the model, we have first studied evaporating drops as steady-state solutions for the case when they are fed through a porous part of the substrate. In particular, an asymptotic analysis has focused on the transition region between the precursor film and the bulk drop; and a numerical continuation of steady-state drops has determined the fully non-linear drop profiles as a function of the overall influx for various values of the length scale ratio ϵ. We have found that for large steady drops, the volume as well as the apparent contact angle decrease for increasing ϵ roughly as $\epsilon^{-1/4}$. This does well agree with the scaling $\epsilon^{-1/4}$ determined via the asymptotic analysis. Note that the mentioned logarithmic corrections to both the overlap range where the matching is done and the resulting profile slope (apparent contact angle) are found to have opposite effects and are too subtle for order-of-magnitude estimates.

Furthermore, we have employed the model to study the time evolution of freely evaporating drops that are not fed through the substrate, i.e., the full evolution equation has been numerically integrated. Thereby the time evolution of several different initial drop shapes (for identical maximal height and volume) has been compared. It has been shown that freely evaporating drops with different initial profiles converge onto certain trajectories in phase space. However, a direct comparison of the freely evaporating drops without influx with the evaporating steady-state drops with influx has shown that the latter cannot be used to approximate the former. A freely evaporating shrinking drop has always a smaller apparent contact angle than the steady drop with influx. Here it has been investigated for a wide range of length scale ratios from $\epsilon = 10^{-6}$ to $\epsilon = 1$. However, as the differences between the two types of profiles slowly decrease with decreasing ϵ, further studies should scrutinise the case of even smaller ϵ.

We have noted that in our simulations the freely evaporating drops with a similar initial geometry (volume and height) to steady-state drops with influx, never spread macroscopically before their contact line starts to recede and the drop shrinks. As drops undergo an initial spreading phase in many experiments, we have investigated this

further and found that drops spread [shrink] from the beginning if their initial contact angle is larger [smaller] than the apparent contact angle of large evaporating drops with influx.

This seems to be a very promising result that should be further scrutinised as it might have interesting consequences: (i) if the apparent contact angle of a steady drop with influx takes the role of an equilibrium contact angle θ_e, relations between the dynamic angles and the contact line velocity known from non-volatile partially wetting liquids [27] could hold. Although, this has recently been shown for the case of evaporating partially wetting liquid [24], it remains an open question for the case of a wetting liquid that we study here. (ii) It might further be possible to predict the maximal drop radius and the contact angle at which the initial spreading ceases, and the 'turn around' to the receding motion occurs. It seems plausible that the profile at turnaround might actually be identical to the steady drop profile with influx at the same volume. Note that the freely evaporating drop spreads *and* evaporates, i.e., the volume at turn-around does not correspond to the initial one.

Note, finally, that here we have studied a particular evaporation model valid for small drops in situations where thermal aspects and the dynamics in the surrounding gas phase can be neglected. However, the non-isothermal models can all be studied with a similar methodology, i.e., the properties of steady drops with local influx can be determined and may be employed to gain a deeper understanding of the coupled transport and phase change processes.

Acknowledgment This study has been supported by the European Union under Grant No. PITN-GA-2008-214919 (MULTIFLOW).

References

1. Leizerson I, Lipson SG, Lyushnin AV (2003) When larger drops evaporate faster. Nature 422:395–396
2. Samid-Merzel N, Lipson SG, Tannhauser DS (1998) Pattern formation in drying water films. Phys Rev E 57:2906–2913
3. Deegan RD (2000) Pattern formation in drying drops. Phys Rev E 61:475–485
4. Deegan RD, Bakajin O, Dupont TF, Huber G, Nagel SR, Witten TA (1997) Capillary flow as the cause of ring stains from dried liquid drops. Nature 389:827–829
5. Huang J, Kim F, Tao AR, Connor S, Yang P (2005) Spontaneous formation of nanoparticle stripe patterns through dewetting. Nat. Mater. 4:896–900
6. Thiele U, Mertig M, Pompe W (1998) Dewetting of an evaporating thin liquid film: heterogeneous nucleation and surface instability. Phys Rev Lett 80:2869–2872
7. Ajaev VS (2005) Spreading of thin volatile liquid droplets on uniformly heated surfaces. J Fluid Mech 528:279–296
8. Anderson DM, Davis SH (1995) The spreading of volatile liquid droplets on heated surfaces. Phys Fluids 7:248–265
9. Cachile M, Benichou O, Cazabat AM (2002) Evaporating droplets of completely wetting liquids. Langmuir 18:7985–7990
10. Pomeau Y (2002) Recent progress in the moving contact line problem: a review. C R Mec 330:207–222
11. Wayner PC (1993) Spreading of a liquid film with a finite contact angle by the evaporation/condensation process. Langmuir 9:294–299
12. Bonn D, Eggers J, Indekeu J, Meunier J, Rolley E (2009) Wetting and spreading. Rev Mod Phys 81:739–805
13. Starov VM, Velarde MG, Radke CJ (2007) Wetting and spreading dynamics. Taylor and Francis, Boca Raton
14. Shahidzadeh-Bonn N, Rafaï S, Azouni A, Bonn D (2006) Evaporating droplets. J Fluid Mech 549:307–313
15. Hocking LM (1995) On contact angles in evaporating liquids. Phys. Fluids 7:2950–2954
16. Poulard C, Guena G, Cazabat A-M, Boudaoud A, Ben Amar M (2005) Rescaling the dynamics of evaporating drops. Langmuir 21:8226
17. Deegan RD, Bakajin O, Dupont TF, Huber G, Nagel SR, Witten TA (2000) Contact line deposits in an evaporating drop. Phys Rev E 62:756–765
18. Dunn GJ, Wilson SK, Duffy BR, David S, Sefiane K (2009) The strong influence of substrate conductivity on droplet evaporation. J. Fluid Mech. 623:329–351
19. Sefiane K, Wilson SK, David S, Dunn GJ, Duffy BR (2009) On the effect of the atmosphere on the evaporation of sessile droplets of water. Phys Fluids 21:062101
20. Lyushnin AV, Golovin AA, Pismen LM (2002) Fingering instability of thin evaporating liquid films. Phys Rev E 65:021602
21. Padmakar A, Kargupta K, Sharma A (1999) Instability and dewetting of evaporating thin water films on partially and completely wettable substrates. J Chem Phys 110:1735–1744
22. Pismen LM (2004) Spinodal dewetting in a volatile liquid film. Phys Rev E 70:021601
23. Rednikov AY, Colinet P (2010) Vapor-liquid steady meniscus at a superheated wall: asymptotics in an intermediate zone near the contact line. Microgravity Sci. Technol. 22:249–255

24. Ajaev VS, Gambaryan-Roisman T, Stephan P (2010) Static and dynamic contact angles of evaporating liquids on heated surfaces. J Colloid Interface Sci 342:550–558
25. Oron A, Davis SH, Bankoff SG (1997) Long-scale evolution of thin liquid films. Rev Mod Phys 69:931–980
26. Thiele U (2010) Thin film evolution equations from (evaporating) dewetting liquid layers to epitaxial growth. J Phys Condens Matter 22:084019
27. de Gennes P-G (1985) Wetting: statics and dynamics. Rev Mod Phys 57:827–863
28. Israelachvili JN (2010) Intermolecular and surface forces. Academic Press, London
29. Kalliadasis S, Thiele U (eds) (2007) Thin films of soft matter. Springer, Wien
30. Ruckenstein E, Jain RK (1974) Spontaneous rupture of thin liquid films. J Chem Soc Faraday Trans II 70:132–147
31. Sharma A (1993) Relationship of thin film stability and morphology to macroscopic parameters of wetting in the apolar and polar systems. Langmuir 9:861–869
32. Thiele U (2007) Structure formation in thin liquid films. In: Kalliadasis S Thiele U (eds) Thin films of soft matter. Springer, Wien, pp 25–93
33. Starov VM, Velarde MG (2009) Surface forces and wetting phenomena. J Phys Condes Matter 21:464121
34. Morris SJS (2001) Contact angles for evaporating liquids predicted and compared with existing experiments. J Fluid Mech 432:1–30
35. Morris SJS (2003) The evaporating meniscus in a channel. J Fluid Mech 494:297–317
36. Doedel E, Keller HB, Kernevez JP (1991) Numerical analysis and control of bifurcation problems (I) bifurcation in finite dimensions. Int J Bifurc Chaos 1:493–520
37. Doedel E, Keller HB, Kernevez JP (1991) Numerical analysis and control of bifurcation problems (II) bifurcation in infinite dimensions. Int J Bifurc Chaos 1:745–772
38. Doedel EJ, Champneys AR, Fairgrieve TF, Kuznetsov YA, Sandstede B, Wang XJ (2000) AUTO97: continuation and bifurcation software for ordinary differential equations. Concordia University, Montreal
39. Thiele U, Neuffer K, Bestehorn M, Pomeau Y, Velarde MG (2002) Sliding drops on an inclined plane. Colloid Surf A 206:87–104
40. John K, Bär M, Thiele U (2005) Self-propelled running droplets on solid substrates driven by chemical reactions. Eur Phys J E 18:183–199
41. Thiele U, Knobloch E (2006) On the depinning of a driven drop on a heterogeneous substrate. New J Phys 8(313):1–37